Technical Report

BEM Static Fire Test Report

Maiden APCP Test Campaign for EUROC

Test Date: March 30, 2026

Authors

Miguel Gómez Macías
Miguel Tejera Lesmes

Propulsion Department
Coheteros Association

Higher Technical School of Engineering
University of Seville

Seville, Spain · April 8, 2026

SUPPORTED BY

Contents

1 Objective

This test represents the maiden static fire of the BEM (Ballistic Evaluation Motor) engine utilizing an Ammonium Perchlorate Composite Propellant (APCP) formulation (AP/HTPB). The primary objective is to acquire high-fidelity, real-world empirical data on the engine's performance with this newly developed propellant.

Analyzing the combustion characteristics of this formulation will allow us to accurately characterize its ballistic properties, refine our internal simulation models, and predict the behavior of future test articles with much higher certainty. Ultimately, this baseline test is a critical step toward securing an optimal, highly reliable propulsion system to fulfill our final objective at the European Rocketry Challenge (EUROC).

2 Motor Configuration

2.1 Configuration Design

Prior to any hot-fire test, extensive simulations are conducted to determine the optimal propellant grain geometry. Both the total propellant mass and the specific grain configuration are strictly tailored to meet the operational objectives of the test.

Designing the motor's internal configuration requires balancing several physical and thermodynamic constraints:

- **Geometric Constraints:** The outer diameter (D_e) of the propellant grains is fixed by the combustion chamber's inner diameter and the thickness of the thermal inhibitor. However, the number of grains and their individual lengths can be modified to achieve the desired burning area evolution.

- **Pressure Boundaries:** Chamber pressure is bounded by a lower and an upper limit. The lower bound is dictated by the propellant's stable combustion threshold; falling below this point drastically reduces efficiency and can induce severe low-frequency combustion instabilities, commonly known as *chuffing*. The upper bound is defined by the mechanical yield strength of the motor casing material. A structural failure due to overpressurization must be avoided at all costs. While higher pressures yield better combustion efficiency, remaining within the safe operational envelope is mandatory.

Given the inherent uncertainties of a maiden APCP test, the BEM (Ballistic Evaluation Motor) engine was selected specifically because it is heavily **over-engineered**. Its structural limits far exceed the expected peak pressures, virtually eliminating the risk of mechanical rupture. Nevertheless, simulations strictly monitor this upper boundary.

Considering these constraints and the main objective, achieving stable combustion to acquire clean sensor data, several trade-off simulations were performed to define the propellant mass, the number of grains, and their dimensions.

The final theoretical configuration comprises **4 BATES grains** with an outer diameter of 58 mm, a core diameter of 25 mm, and a length of 90 mm. These specifications are summarized in Table 1:

In addition to grain geometry, the nozzle throat diameter acts as the primary choke point, drastically influencing chamber pressure. For this test, the nozzle throat diameter was machined to **12.9 mm** ($D_{nozzle} = 12.9$ mm).

Number of Grains (BATES)	4
Outer Diameter (D_e)	58 mm
Core Diameter (d_{core})	25 mm
Length (L)	90 mm
Propellant Mass (m_{prop})	1201 g

Table 1: Theoretical propellant grain configuration.

2.2 Propellant Manufacturing

The propellant utilized for all testing campaigns is manufactured and processed entirely in-house by the association's Propulsion Department.

Once the required propellant mass was determined via simulation, the specific quantities of the APCP constituents were prepared. The manufacturing procedure follows a strict internal protocol: mold preparation, precise mixing of components, vacuum degassing (to eliminate internal voids that could cause combustion instabilities), casting the slurry into the molds, and curing.

Once fully cured and demolded, the actual dimensions and densities of the grains are measured to account for manufacturing deviations from the theoretical model. Table 2 presents the as-built length and density ratio (ρ_{real}/ρ_{ideal}) for each grain. Diameters remain constant as they are constrained by the casting molds.

BATES Grain	**1**	**2**	**3**	**4**
Length (L) [mm]	90.9	90.2	88.2	91.2
Density Ratio	0.969	0.942	0.973	0.966

Table 2: As-built physical properties of the manufactured APCP grains.

The density ratio is measured once the propellant grain is removed from the mold; however, this value is subject to minor adjustments during the preparation of the report.

These empirical values are subsequently fed back into the simulator to generate an accurate, "as-built" predictive model of the static fire test.

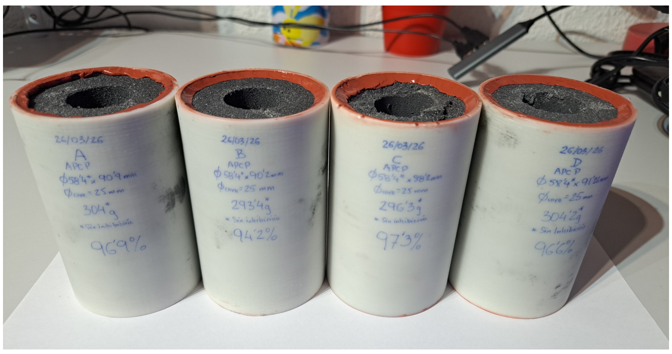

Figure 1: Manufactured BATES grains with their physical characteristics labeled on the inhibiting surface.

2.3 Risk Assessment

This section outlines the primary risks associated with both the manufacturing process and the static fire operation.

Manufacturing Risks: APCP manufacturing involves handling chemical components that emit potentially toxic fumes. Consequently, all personnel involved in the active mixing phases are required to use appropriate Personal Protective Equipment (PPE) to mitigate inhalation risks. Furthermore, the curing phase is critical; the final viscosity and structural integrity of the grain dictate its viability. Improper curing or binder formulation issues can lead to structural anomalies such as internal voids, bubbles, or cracks. This risk is mitigated by strictly controlling mixture additives and the curing profile.

Operational Risks: During the hot-fire test, a primary risk is *anomalous combustion*, often linked to manufacturing defects such as internal voids or cracks, which can exponentially increase the burning surface area and lead to aggressive overpressurization. Additionally, data acquisition is subject to operational risks, specifically the manual calibration required for the load cell and the dynamic mechanical oscillations of the test bench base, both of which can introduce artifacts into the sensor measurements. Another significant risk is a major deviation between empirical data and simulation predictions (either severe underperformance or overpressurization). Should this occur, it will be treated as a critical learning opportunity to recalibrate our internal models.

Thermal Risks: APCP burns at extremely high temperatures. In this specific setup, the BEM motor (made of A304 stainless steel) operates with a thermal liner, albeit a highly inefficient one for this propellant class. Due to the inadequacy of this insulating layer against APCP heat fluxes, the hardware is subjected to immense thermal loads. While the stainless steel casing is robust enough to survive, the nozzle is highly susceptible to severe erosion and melting. Consequently, only the nozzle is considered a single-use test article for this specific APCP campaign, whereas the rest of the motor remains reusable.

2.4 Simulation Results

Table 3 summarizes the critical performance parameters predicted by the simulation, using the as-built geometrical and physical properties of the propellant grains. Values have been appropriately rounded for engineering clarity.

Max Chamber Pressure (P_{max})	55.0 bar
Max Thrust (E_{max})	97.4 kg
Burn Time ($t_{burning}$)	2.89 s
Total Impulse (I_t)	2541 Ns
Specific Impulse (I_{sp})	203 s

Table 3: Predicted performance parameters based on "as-built" simulation.

In addition to these numerical parameters, other performance metrics are obtained, though they are secondary when evaluating the theoretical baseline of the motor. To ensure maximum reliability and mitigate simulation bias, these results were cross-verified using two independent, internally developed simulation tools: **HERMES** and **EDISON**. Both proprietary tools provided highly correlated theoretical outputs.

3 Instrumentation

Characterizing a solid rocket motor powered by APCP propellant presents a critical challenge in data acquisition. The extreme temperatures, violent ignition transients, and harsh vibrational environment demand a measurement system that is robust, high-speed, and entirely free of electrical interference.

For this static fire test, the instrumentation architecture was designed not merely to record data, but to **survive and operate with precision** under borderline conditions, accurately digitizing the thermodynamics, acoustics, and structural response of the BEM engine.

3.1 Data Acquisition: Dewesoft SIRIUS i-CHG

The core of our measurement system is the **Dewesoft SIRIUS i-CHG** data acquisition (DAQ) system. This high-performance hardware provides 8 analog channels with full galvanic isolation, allowing for the simultaneous integration of transducers with varying signal natures (piezoelectric, IEPE, voltage) without the risk of ground loops or electrical noise.

Given the inherent complexities of open-field testing, the system's operability was structured upon three fundamental pillars:

- **Isolated Power Supply:** The hardware operates via alternating current (AC) supplied by a portable power generator, completely isolating the test platform from any public power grid.
- **Secure Remote Control:** The DAQ is linked via a direct interface to a laptop located in the control bunker, guaranteeing real-time telemetry monitoring from a safe distance.
- **Real-Time Mathematics:** Rather than relying exclusively on heavy, post-test external processing, the *DewesoftX* software allows us to execute algorithms (*Math Channels*) directly on the raw signal. This is vital for visualizing parametric conversions, root mean square (RMS) values, or spectrograms (STFT) during the very millisecond the test is occurring.

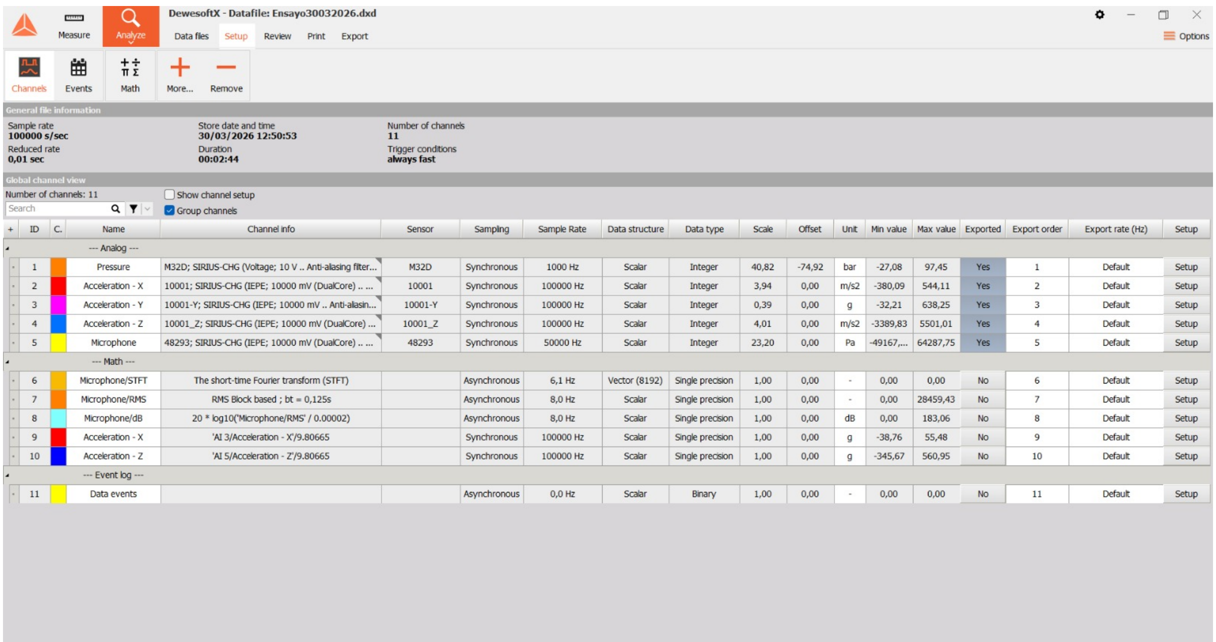

Figure 2: General *Channel Setup* configuration within the DewesoftX environment. Parametric assignments and individualized sampling rates per sensor are displayed.

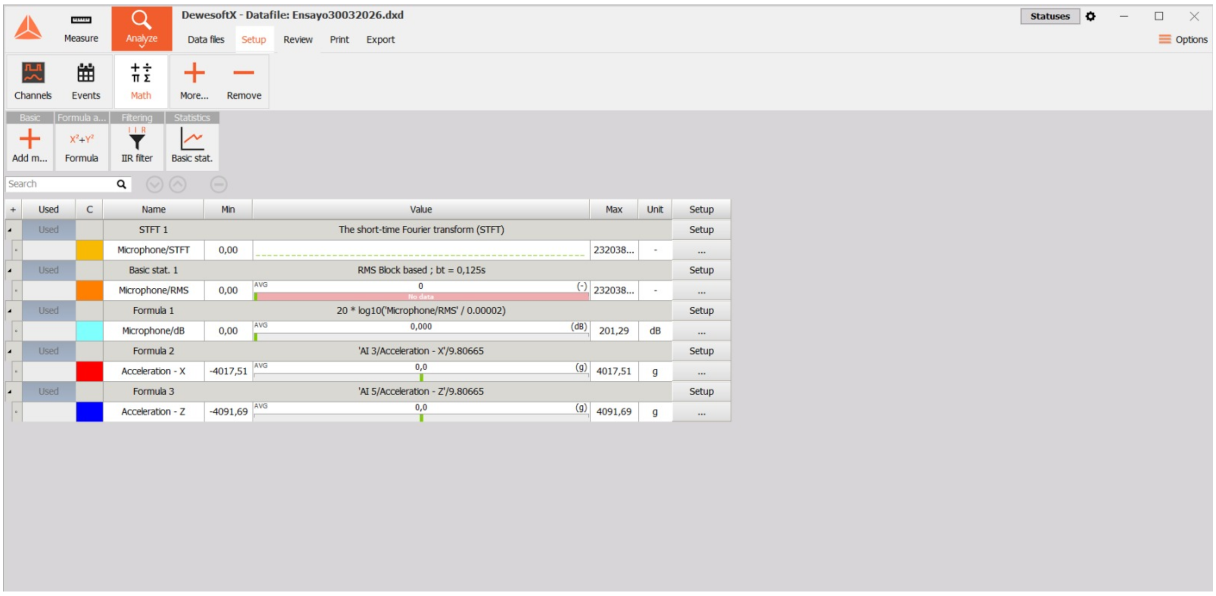

Figure 3: DewesoftX Mathematics module operating live for the parametric processing of acoustic signals.

3.2 DAQ Sensor Configuration

Our software configuration philosophy was straightforward: **assign individualized sampling rates** for each transducer. By avoiding blanket over-sampling, we optimize computational load while ensuring every physical phenomenon strictly complies with the Nyquist Theorem.

3.2.1 Pressure Sensor

Recording chamber pressure is the most critical thermodynamic parameter. However, APCP ignition generates a ballistic transient shock so violent that the primary risk to data acquisition is **channel overload (*clipping*)**. If the analog-to-digital converter (ADC) saturates, the signal is permanently contaminated with unrecoverable noise.

To guarantee the integrity of the pressure curve, the channel was configured under three strict directives aimed at maximum stability:

1. **Capped Sampling Rate (1,000 Hz):** Instead of pushing for extreme frequencies, we capped the rate at 1 kHz. This is the optimal threshold to capture the macroscopic dynamics of chamber pressure without recording the parasitic "white noise" intrinsic to high-velocity gas flow.

2. **Fixed Voltage Range (10 V):** Given that the sensor requires an excitation voltage between 9 and 32 V, we rigidly anchored the analog reading range to 10 V. More sensitive scales (e.g., 0.5 V) would have amplified the ignition shock, instantly saturating the system.

3. **Deactivation of *DualCoreADC®*:** While this Dewesoft technology is exceptional for maximizing dynamic range in stable environments, its auto-adjusting nature (alternating between high and low gain scales) is counterproductive during impulsive events. By disabling it, we forced a rigid, unwavering scale during the critical transient phases.

3.2.2 Accelerometry (IEPE)

To characterize the vibrational profile, we implemented an Endevco 66N7 triaxial piezoelectric accelerometer. In the software, the Z-axis was aligned with the axial vibrations (thrust vector), while the X and Y axes captured radial components.

- **Extreme Sampling (100,000 Hz):** To accurately discriminate the structural impact of ignition (*shock*) from potential high-frequency acoustic combustion instabilities (> 1000 Hz), the sampling rate was elevated to the necessary limit.

- **Coupling and Calibration:** The channels were configured in IEPE mode with a high-pass filter (AC coupling) enabled to eliminate direct current *offset*. Due to a read incompatibility with the sensor's TEDS chip, the factory-calibrated pure sensitivities were introduced manually (X-Axis: 2.489 mV/g; Y-Axis: 2.578 mV/g; Z-Axis: 2.444 mV/g).

3.2.3 Free-Field Microphone

Capturing the acoustic signature of an APCP plume without destroying the sensor required a PCB Piezotronics 130F20 array condenser microphone. Its pre-amplified ICP® technology allowed the signal to be channeled losslessly through coaxial cable runs exceeding 20 meters.

- **Acoustic Configuration:** With a rate of 50,000 Hz, we covered the entire audible spectrum (up to 20 kHz) while strictly avoiding *aliasing*. By setting the analog range to 10 V, we established an acoustic measurement ceiling of approximately 141 dB.

- **Live Monitoring:** Utilizing the math engine, we programmed the immediate visualization of the Overall Sound Pressure Level ($20 \cdot \log_{10}(RMS/0.00002)$) and a 3D STFT (Short-Time Fourier Transform) thermal map to observe the evolution of audible tones generated by the exhaust gases.

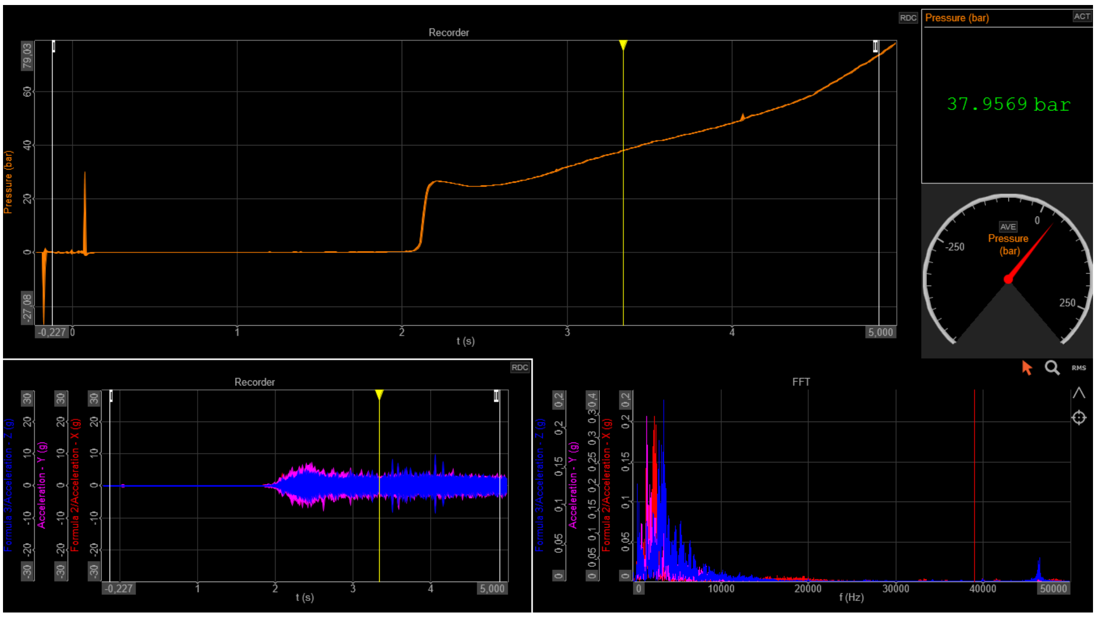

Figure 4: *Dashboard 1*: Real-time parametric history of chamber pressure (orange) and triaxial accelerometric response.

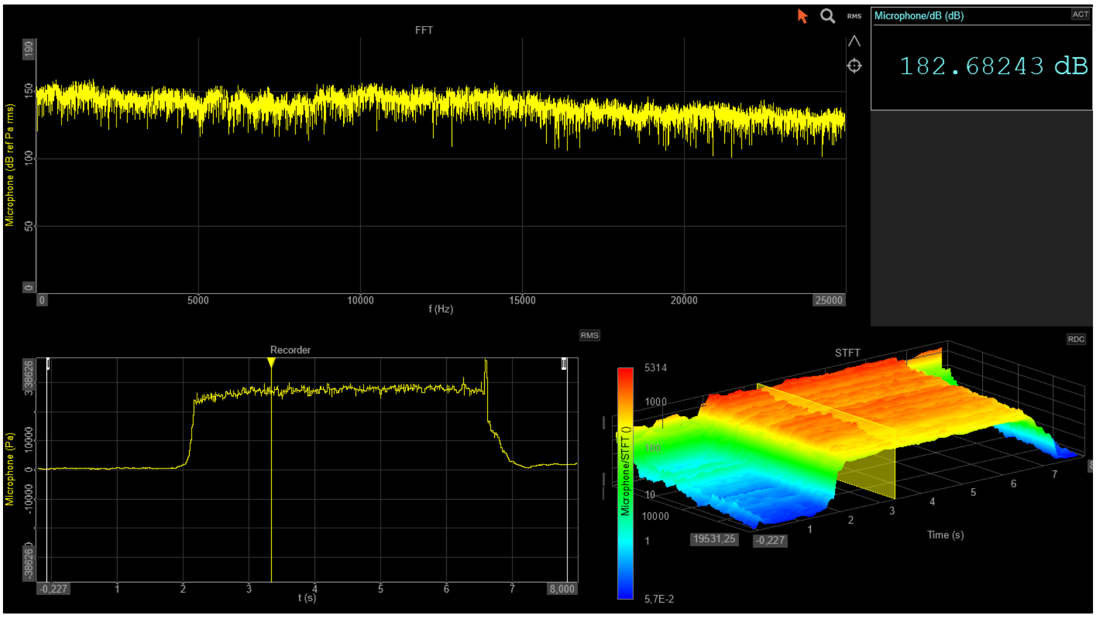

Figure 5: *Dashboard 2*: Frequency analysis. Displays the acoustic FFT analyzer and the 3D STFT spectrogram generated by the supersonic plume shear.

3.2.4 Load Cell

The direct measurement of thrust, the ultimate performance parameter of the engine, is conducted using an **independent and dedicated** data acquisition system that operates in parallel with the Dewesoft instrumentation.

The transducer is a strain gauge load cell installed at the structural base of the test bench. Its operating principle relies on an internal **Wheatstone bridge**. The force exerted by the motor deforms the strain gauges, causing a resistance imbalance within the bridge. This imbalance generates a voltage signal that is directly proportional to the applied force.

Due to the vertical configuration of the test bench (with the nozzle pointing upwards), the entirety of the engine's thrust is translated into a **pure compressive load** on the cell. The data acquired by this system is therefore fundamental to obtaining the true thrust curve over time, which will subsequently be correlated with the chamber pressure profile for a comprehensive performance validation.

4 Test Operations

4.1 Setup and Preparation

This section outlines the pre-test preparations and the physical layout of the various components, including the test article, the sensor suite, and the data acquisition hardware.

4.1.1 Motor Assembly

The procedure begins with the insertion of the APCP propellant grains, encased in a **liner**, into the motor casing. The fully loaded engine is then securely mounted and aligned on the test stand platform.

Once the mechanical integration is complete, the sensor suite must be fully installed and calibrated on both the test stand and the motor. Strictly following safety protocols, the pyrotechnic igniter is inserted through the nozzle and connected to the external ignition system battery **only as the final step** before clearing the pad. This ensures maximum safety for the engineering team prior to authorizing the ignition sequence.

4.1.2 Physical Sensor Layout

The most advanced hardware in the world is useless if its physical positioning is incorrect. The geometric installation of the instrumentation was meticulously planned to maximize signal fidelity and protect the equipment from the destructive test environment:

- **Pressure Transducer at the *Aft Closure*:** Breaking with the traditional configuration of placing the sensor at the forward closure, we tapped it directly into the structural interface with the nozzle. *The rationale?* To record the pure static thermodynamic pressure of the gases right at the convergence zone, eliminating dead volumes that could attenuate the reading of rapid transients.

- **Accelerometry on the Test Stand:** The transducer was not mounted on the motor casing, but rigidly anchored to the wooden base, adjacent to the load cell (which is operated by an independent DAQ). Our goal here is **dynamic compensation**: characterizing the resonance and elasticity of the wooden structure. During post-processing, this vibrational "footprint" will allow us to mathematically isolate the engine's true thrust from the mechanical oscillations of the stand.

- **Oblique-Angled Microphone:** Located at the mandatory safety distance (> 20 meters), the microphone **does not point directly at the nozzle**. It was oriented with an upward angle toward the exhaust plume's expansion zone. This provides a clean far-field acoustic irradiation reading and prevents the frontal shockwave and ejected APCP slag from impacting the sensor diaphragm and causing signal saturation.

Figure 6: Dewesoft SIRIUS i-CHG deployed in the field. Note the coaxial connections and BNC connectors, which are critical for rejecting electromagnetic interference (EMI) in the test environment.

Figure 7: Remote monitoring station located outside the hazard zone. The decentralized architecture ensures human control and real-time parametric visualization without compromising safety.

Figure 8: Image of the test running

Once this step is completed, we are fully prepared to commence the test. Therefore, after mounting the engine and the sensors, the necessary safety measures are taken (establishing a safe distance from the engine and ensuring adequate protection), and we proceed with ignition (Figure 8).

5 Data Analysis and Results

The primary operational conclusion of the test is the **exceptional quality of the raw signal**, which is a direct testament to the robustness of the instrumentation setup. The need for post-processing was minimal, allowing for a direct analysis of the physical magnitudes recorded by the Dewesoft system.

5.1 Chamber Pressure Curve

The chamber pressure profile, shown in Figure 9, is the key performance indicator. The curve required no filtering and displays the classic behavior of a BATES configuration utilizing APCP propellant:

- A clean and abrupt **ignition transient** at t $\approx$ 2.0 s.
- A **progressive burn phase**, where pressure rises steadily as the propellant is consumed and the internal burning area of the grains increases, reaching a maximum of **97 bar**.
- A sharp **tail-off** (combustion cutoff), indicative of a complete and homogeneous consumption of the propellant.

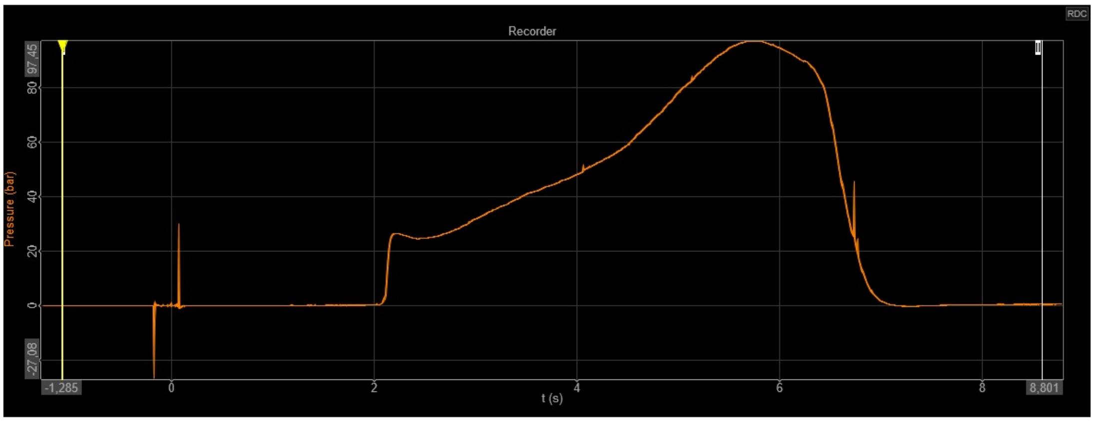

Figure 9: Temporal profile of the chamber pressure. The signal's clarity allows for the distinct identification of all combustion phases.

5.2 Thrust Curve

Thrust is measured using a load cell against which the motor pushes during operation. Since pressure and thrust are intimately coupled variables, their curves should exhibit similar behavior. In this instance, due to structural vibrations present in the test platform, the raw data measured by the load cell was filtered to mitigate oscillations. The resulting curve is presented below:

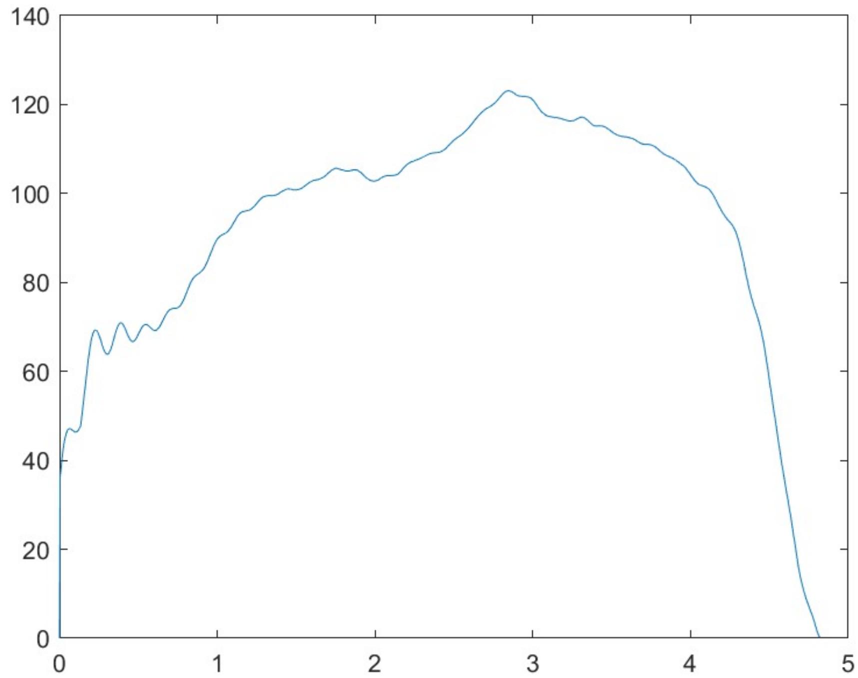

Figure 10: Evolution of the thrust generated by the motor.

The X-axis represents time, and the Y-axis represents thrust in kilograms. Similar to the pressure representation, the graph shows a progressive profile, where thrust increases until it reaches a maximum peak of **123.8 kg** before dropping rapidly.

5.3 Vibrational Characterization

The FFT analysis of the accelerometer (Figure 11) reveals that the vibrational energy of the test stand is concentrated primarily in the **low-frequency band ($<$ 5,000 Hz)**, which is characteristic of a mechanical structural response.

The most relevant finding is that the peaks of highest vibrational amplitude coincide with the onset of the pressure rise, confirming a **direct correlation between the motor's load and the structure's response**. Crucially, the absence of discrete high-frequency tonal peaks confirms a stable combustion, free of resonant instabilities.

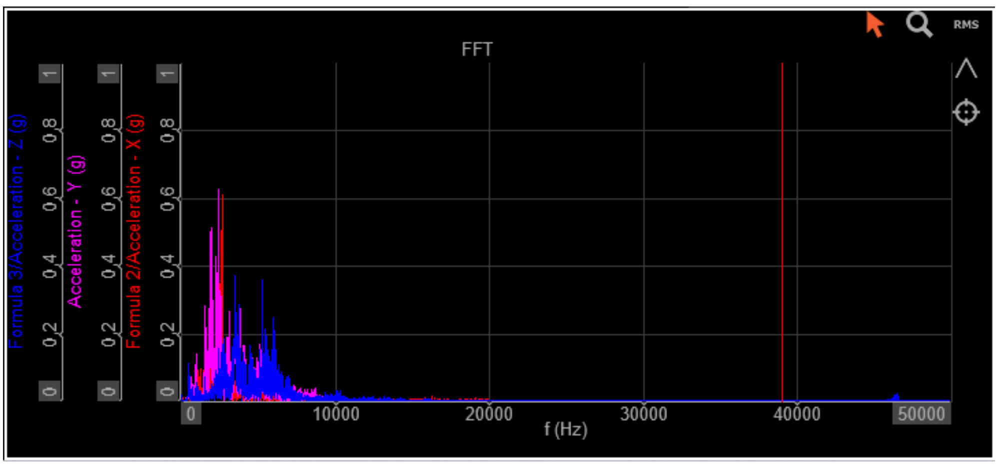

Figure 11: Fast Fourier Transform (FFT) analysis of the accelerometer signal during the phase of maximum vibration.

5.4 Acoustic Signature Analysis

The acoustic signature of the motor provides a clear insight into the stability and energy of the combustion process.

- **Temporal Analysis:** The raw signal in Pascals (Figure 12a) shows a **stable acoustic pressure plateau** throughout the entire burn. This constancy is a direct indicator of sustained thrust and homogeneous combustion.
- **Time-Frequency Analysis (STFT):** The 3D spectrogram (Figure 12b) visually corroborates this stability. It displays a **broadband** energy distribution, characteristic of *supersonic jet noise*, which remains constant from ignition to shutdown. This conclusively rules out the presence of evolutionary acoustic instabilities.

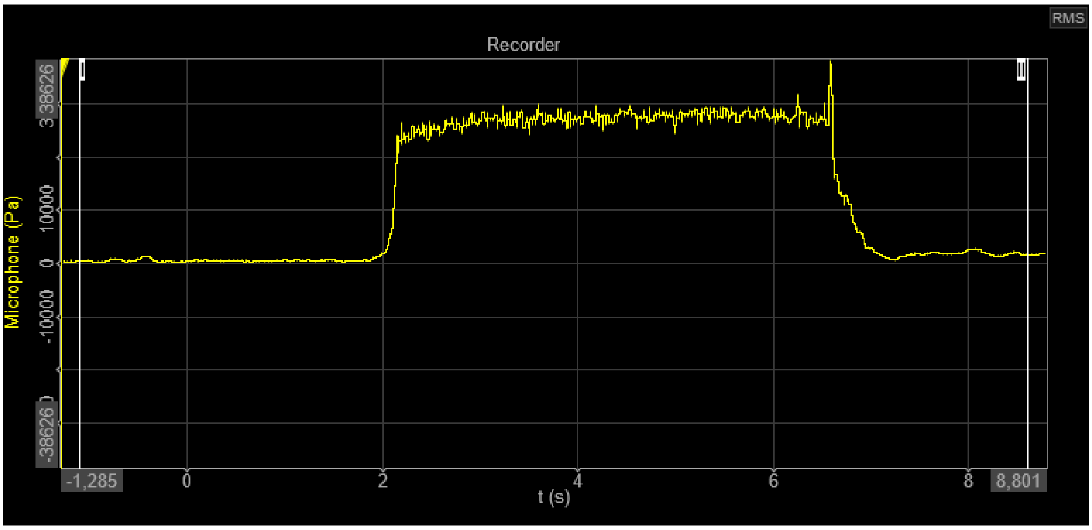

(a) Temporal microphone signal in Pascals, showing a stable plateau.

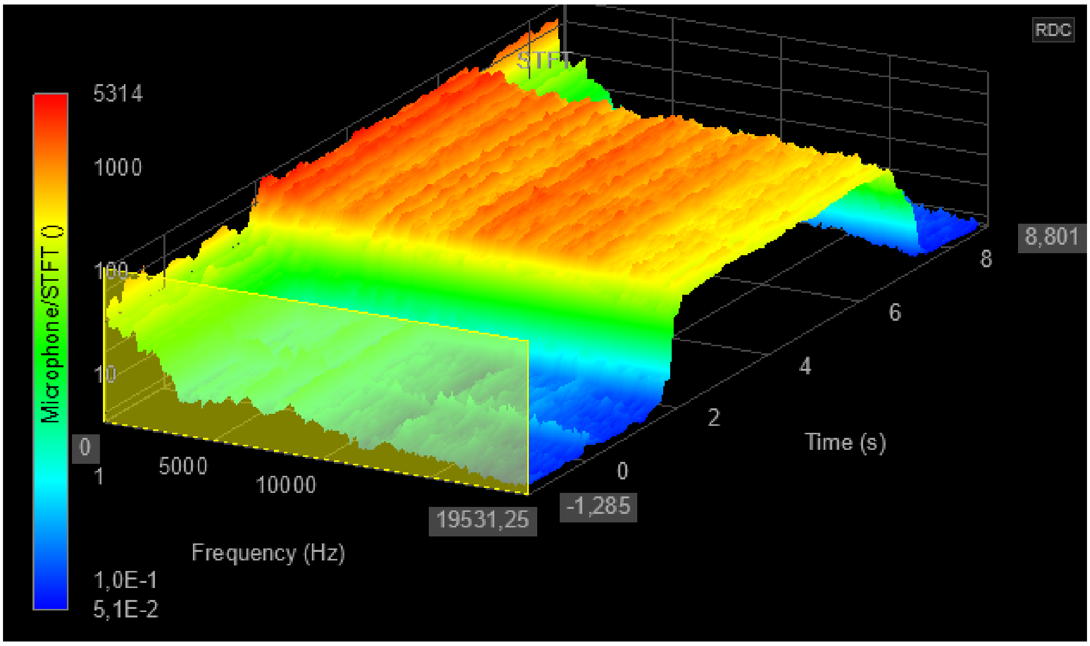

(b) Spectrogram (STFT) confirming the broadband nature and temporal stability of the acoustic signature.

Figure 12: Analysis of the acoustic signal in both time and frequency domains.

5.5 Motor inspection

After the test, once the motor has cooled down, a thorough inspection of the engine and all its components is conducted to draw further conclusions and assess whether any damage has occurred.

First, an external visual inspection is performed, with particular attention paid to the bolted joints connecting the nozzle and the forward closure to the combustion chamber casing. During this initial examination, no anomalies are observed.

Following this step, the motor is disassembled into its three primary sections: the aft closure, the nozzle, and the combustion chamber:

- **Aft closure:** This is the component least prone to failure or degradation. A rapid visual inspection is conducted to check for any noticeable defects, and it is found to be in perfect condition. A more detailed examination is performed on the O-rings, which are responsible for ensuring the motor's hermetic seal. The objective is to identify any defects or tears; however, they remain in good condition and can be reused in subsequent tests.

Figure 13: Aft closure of the motor after the test.

- **Nozzle:** As previously mentioned, this is one of the most critical components due to the extreme operating temperatures. Surprisingly, absolutely no throat erosion or geometric degradation is observed in the nozzle, which is considered a major success for the hardware design. Both the divergent and convergent sections were thoroughly examined. The throat appears slightly obstructed due to the deposition of combustion slag. This residue is also present throughout the rest of the nozzle's internal surface. Specifically, a very hard crust is observed in the convergent section (Figure 14a). While this will be analyzed in greater depth, it appears to be molten aluminum slag originating from the propellant formulation. Finally, as with the closure, the O-rings are inspected and confirmed to remain in nominal condition, maintaining a perfect pressure seal.

(a) Nozzle with the aluminum layer in the convergent section

(b) Clean nozzle where the aluminum layer has been removed

Figure 14: Nozzle after the test

- **Combustion chamber:** Inside the combustion chamber are the propellant grains, which are covered by inhibitors and entirely encased within a liner. The inspection aims to examine the remnants of these elements and evaluate their structural integrity. The liner exhibits no significant deformation and remains in a single contiguous piece; that is, it has not ruptured, nor have any fragments detached. The end inhibitors, those corresponding to the grains closest to the nozzle and the closure, exhibit greater deformation than the two central ones. Nevertheless, no material shedding has occurred.

Figure 15: Liner, nozzle, nozzle's O-rings, combustion chamber and removed aluminum crust

Overall, the motor casing and hardware remain in excellent condition. Notably, the nozzle has withstood the full thermal load of the test without any thermal protection or ablative coating. Therefore, the entire motor assembly is considered fully flight-ready and can be reused for the subsequent test campaign without hardware replacements.

6 Conclusions and Future Work

6.1 Conclusions

This static fire test was a resounding success, meeting its objectives satisfactorily and representing a pivotal milestone for Coheteros. We have simultaneously validated our internally manufactured APCP formulation and, critically, our advanced instrumentation architecture centered around the Dewesoft SIRIUS system. The exceptional quality of the acquired data establishes a highly reliable operational baseline and provides the "ground truth" necessary to rigorously refine our "HERMES" and "EDISON" simulation software.

Despite the overall success of the test, certain performance metrics deviated from expectations. While both thrust and pressure outputs were strong, confirming excellent overall rocket motor performance, there are significant discrepancies compared to the simulations. Specifically, the empirical efficiency exceeded 100% relative to the theoretical models. While we suspect this anomaly stems from the thrust sensor's calibration and measurement, a deeper analysis is required. Consequently, further testing is necessary to analyze these variations, align our theoretical models with real-world data as closely as possible, and ensure consistent repeatability.

In conclusion, this test represents a turning point for the association. Numerous milestones were achieved successfully for the first time, ranging from manufacturing relatively large quantities of propellant to acquiring real test data in a highly professional and precise manner. Because of this, we have full confidence in our methodologies and are on the right track to achieving our ultimate goals.

6.2 Future Work: The Static Thrust Challenge

One of our immediate post-test objectives focuses on validating and improving the propellant manufacturing process. The goal is to automate it as much as possible to prevent major discrepancies between tests and eliminate potential issues during any phase of production. Furthermore, we aim to optimize the APCP composition to create a formulation that is easier to handle, poses fewer manufacturing challenges, and yields the best possible properties to optimize combustion and increase specific impulse.

For our upcoming tests, we will integrate our new **Kistler piezoelectric force sensor** to perform high-fidelity thrust measurements. This is where the advanced processing capabilities of DewesoftX will give us a decisive competitive advantage.

The Challenge: Measuring a sustained, static force with a piezoelectric sensor is physically challenging due to the inherent phenomenon of **signal drift**. The electrical charge generated by the sensor naturally leaks over time, an effect accelerated by the AC-coupling high-pass filter of the charge amplifier. This causes the measured signal to decay exponentially towards zero, even when the engine's thrust is constant. The conventional industry solution involves purchasing expensive, specialized quasi-static charge amplifiers.

Our Solution: Hardware-Smart Software. Instead of relying on additional hardware, our approach leverages the raw power of the SIRIUS-i CHG electronics combined with advanced mathematical compensation in DewesoftX. As detailed in our internal validation report[1], we have implemented and experimentally verified a reconstruction algorithm based on the exact analytical inversion of the hardware's first-order high-pass filter.

This method applies a **temporal integration compensation** that mathematically reconstructs the charge lost by the filter, sample by sample.

- **Result:** A perfectly flat and stable thrust curve that is 100% faithful to the real performance of the motor.
- **Advantage:** A massive optimization of resources, solving a fundamental physical limitation purely with intelligent software and avoiding significant investment in intermediate hardware.

This methodology is already validated. The next step is its full-scale implementation in our test bench. The upcoming static fire tests promise to deliver the most precise and reliable pressure and thrust curves we have ever obtained. The best is yet to come.

[1] Reference document: "Medición de Fuerza Estática con Sensores Piezoeléctricos -Sistema Kistler / Dewesoft", M. Tejera Lesmes, Propulsion Dept. - Coheteros.